



University of Tennessee, Knoxville  
**TRACE: Tennessee Research and Creative  
Exchange**

---

Chancellor's Honors Program Projects

Supervised Undergraduate Student Research  
and Creative Work

---

5-2022

## **Defining Interactions Between Deformable DNA Origami and Lipid Bilayers Through Molecular Dynamics Simulation**

Zachary A. Loyd

University of Tennessee, Knoxville, [zloyd@vols.utk.edu](mailto:zloyd@vols.utk.edu)

Follow this and additional works at: [https://trace.tennessee.edu/utk\\_chanhonoproj](https://trace.tennessee.edu/utk_chanhonoproj)

 Part of the [Biophysics Commons](#), [Biotechnology Commons](#), [Membrane Science Commons](#), and the [Other Biochemistry, Biophysics, and Structural Biology Commons](#)

---

### **Recommended Citation**

Loyd, Zachary A., "Defining Interactions Between Deformable DNA Origami and Lipid Bilayers Through Molecular Dynamics Simulation" (2022). *Chancellor's Honors Program Projects*.  
[https://trace.tennessee.edu/utk\\_chanhonoproj/2506](https://trace.tennessee.edu/utk_chanhonoproj/2506)

This Dissertation/Thesis is brought to you for free and open access by the Supervised Undergraduate Student Research and Creative Work at TRACE: Tennessee Research and Creative Exchange. It has been accepted for inclusion in Chancellor's Honors Program Projects by an authorized administrator of TRACE: Tennessee Research and Creative Exchange. For more information, please contact [trace@utk.edu](mailto:trace@utk.edu).

# **Defining Interactions Between Deformable DNA Origami and Lipid Bilayers Through Molecular Dynamics Simulation**

**Zachary Loyd**

Biochemistry & Cellular and Molecular Biology

University of Tennessee, Knoxville

**Faculty Advisor:** Steven Abel (sabel1@utk.edu)

**Graduate-Student Mentor:** Nikhil Nambiar

Chemical and Biomolecular Engineering

University of Tennessee, Knoxville

## **ABSTRACT**

DNA origami is a relatively new form of nanotechnology that utilizes DNA complementarity to create self-assembled 3D structures. Recent developments have used this technology to create flexible nanoscale structures with tunable mechanical properties. The capacity for deformation in nanoparticles opens many new and intriguing possibilities for precise control over their interactions with the environment. These techniques have been applied for a variety of purposes, but DNA origami interactions with membranes have still only been investigated with rigid nanoparticles. Considering the importance of particle-particle interactions in inducing membrane curvature, which is critical for many cellular processes, it is imperative that the study of deformable DNA origami nanoparticles be expanded to investigate interactions with membranes. We have utilized coarse-grained molecular dynamics simulations to characterize how deformable DNA origami hinges behave when adsorbed to a membrane by cholesterol anchors. We found that the hinges could induce membrane curvature, and their ability to do so changed with their stiffness. The membrane deformations caused by these particles also encouraged the hinges to aggregate, potentially laying the groundwork for the design of useful self-assembling behaviors between nanoparticles — something that is seen in natural membrane sculpting proteins.

## 1. BACKGROUND AND INTRODUCTION:

DNA origami is a method of bottom-up, nanoscale self-assembly that has shown great promise in a variety of applications<sup>11,14</sup>. Origami structures are typically created from the hybridization of one long single-stranded DNA (ssDNA) scaffold and a collection of shorter ssDNA staples. By carefully designing the sequences of these strands, custom, complex, 3D structures can self-assemble at the nanometer scale<sup>11</sup>. This technique has been employed previously to create long fibers that ‘molecular spider’ nanorobots can walk upon<sup>3</sup>, designs for potential reversible anticoagulant drugs for hemodialysis patients<sup>1</sup>, and possible biosensors and drug carriers that can target cancer cells<sup>9</sup>. DNA origami has even been used to create nanorobots that can detect and respond to protein cues within a living cockroach, creating functional logic gates that can perform basic computations<sup>17</sup>.

Typical applications of DNA origami have focused primarily on the design of rigid structures, but methods have recently been developed to create origami nanostructures that are non-rigid with programmable mechanical properties. This can be accomplished by implementing non-hybridizing sequences on the scaffold strand, creating ssDNA portions of the origami that remain flexible<sup>14</sup>. This technique has been utilized to create simple mechanisms with 1D, 2D, and 3D motion, including a hinge with its joint made from ssDNA<sup>14</sup>. Further, implementation of flexible sequences allows origami deformation to be induced by outside stimuli. For example, the addition of “locking strands” that will hybridize to previously flexible ssDNA, making it more rigid, can drive the motion of origami structures<sup>15</sup>. Other techniques have been used to create a DNA origami Möbius strip that could expand to twice its size, triggered by a ‘strand displacement’ mechanism<sup>10</sup>.

One of the most significant applications of DNA origami is the creation of biomimetic structures. Predicting protein folding based on amino acid sequence alone is a notoriously difficult problem, rendering the synthesis of custom proteins from scratch an unviable method. It is viable, however, to design DNA origami from the bottom up, then modify the structure with attachments mimicking what could be found on an analogous protein<sup>3</sup>. Origami mimics of BAR-domain proteins have been utilized to sculpt curvature in phospholipid membranes<sup>13</sup>. BAR proteins are banana-shaped dimers that adsorb to membranes, inducing curvature and promoting the formation of common cellular membrane structures such as folds and tubes<sup>13</sup>. These processes are fundamental to the function of cells and are therefore particularly intriguing to replicate bottom-up with DNA origami.

Particles adsorbed to membranes participate in a complex ecosystem of interactions with each other, often by means of inducing local curvature to recruit or elicit responses from other particles<sup>13,19</sup>. These interactions can have significant cascading effects, resulting large-scale changes to the local environment. Considering the importance of inducing membrane curvature, it is interesting to explore the possibility of incorporating the capacity for deformation into a particle that could adsorb onto and deform a membrane. Despite the promise of this route of investigation, it is, at the time of writing, almost entirely unexplored. One DNA origami structure developed by Franquelim, et al. was convex in shape, with cholesterol moieties attached along its edge to allow for adsorption to a membrane<sup>13</sup>. We have applied a similar design approach to a simulated, coarse-grained model based on the deformable DNA origami hinges created by Marras, et al<sup>14</sup> in hopes to pave a way into this new field of study.

A computational approach to studying DNA origami allows for observations to be made that would be otherwise be difficult or impossible in vitro. Analyzing the angles of origami

hinges with microscopy, for example, is troublesome on its own<sup>14</sup>, and likely not feasible when adsorbed to a membrane. By using molecular dynamics simulations, individual particles and their interactions with membranes can be observed in detail. All-atom simulations would be too computationally expensive to be used effectively, but well-characterized coarse-grained force-fields allow for these larger systems to be simulated without excessive sacrifice to accuracy<sup>16</sup>. Simulation also allowed us to observe complex interactions that occurred between origami, perform analysis of the system's energetics via umbrella sampling methods, and precisely modify attributes of the origami with ease.

## 2. METHODS

Our molecular dynamics simulations were performed using the GROMACS simulation package v5.1.2 and MARTINI force field v2.2 with standard MARTINI parameters for non-bonded interactions<sup>16,12</sup>. The LINCS algorithm was used for bonded interactions. The van der Waals interactions were modeled using a Lennard-Jones potential, truncated at 1.1 nm using the potential-shift-Verlet cut-off scheme. Coulombic interactions were truncated at 1.1 nm as well, using the reaction field method.

The DNA origami hinge model (*Fig. 1*) was developed by constraining 6 MARTINI cholesterol molecules with bonds between their respective RO1 beads. These molecules were organized in parallel sets of three, creating two symmetrical V-

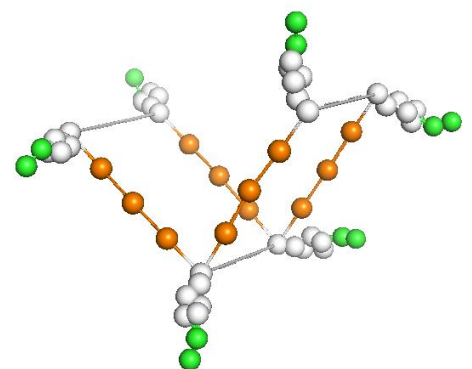


**Figure 1:** The simulated DNA origami hinge model. The orange beads are Q0 type MARTINI beads, and the white and green beads are the attached cholesterol molecules.

shapes offset by 3 nm. There are 3.2 nm between each cholesterol molecule within the same V-shape. The negatively charged Q0 type MARTINI beads connect between each pair of cholesterols, forming the arms of the hinge. This is meant to represent the phosphate backbone of a DNA helix. The 90° resting angle of the hinge is set by a cosine-based angle potential from the GROMOS-96 force field. The force constant ( $k_\theta$ ) for this potential is varied throughout the simulations from 50 kJ mol<sup>-1</sup> to 500 kJ mol<sup>-1</sup>. All simulations used periodic boundary conditions to minimize effects of the boundaries.

For the simulations with the origami hinge(s) adsorbed to the phospholipid bilayer, CHARMM-GUI MARTINI maker was used to construct a solvated bilayer of 1:1 DOPC to DPPC molecules, which are varieties of phosphatidylcholine lipids<sup>2,4-8</sup>. Standard MARTINI models for these lipid types were used. The hinge was randomly inserted into the system, replacing water beads, and guided to interface with the bilayer using a variety of steered simulations. Energy minimization and equilibration steps were performed both after the hinge was initially inserted and after it adsorbed. Energy minimization was performed for 10,000 steps using the steepest descent algorithm with restraints. Equilibration occurred in 5 steps, increasing the time step from 2 fs to 20 fs over a total of 900,000 steps, 4750 ps. Velocity rescale thermostat temperature coupling was used with a reference temperature of 303.15 K and three temperature groups: the water beads, the hinge, and the membrane lipids. Semiisotropic Berendsen pressure coupling was also used with a reference pressure of 1 bar and a compressibility  $K_z = K_{xy} = 3 \times 10^{-4}$  bar<sup>-1</sup>. After the origami adsorbed and equilibrated, production simulations were run for a total of 2  $\mu$ s with similar parameters to the equilibration steps, except with Parrinello-Rahman barostat pressure coupling, using the final 1  $\mu$ s of simulation for analysis to ensure complete equilibration was achieved.

The system for the simulations with a single hinge on the bilayer consisted of 336 lipids, 1 DNA origami hinge, and 6718 water beads. The simulations with two hinges required a larger system of 1332 lipids, 2 hinges, and 41,088 water beads.

Simulations of the hinge in water without a bilayer were equilibrated via the same methods described above but instead using two temperature groups for the temperature coupling: the water beads and the hinge. The hinge was solvated with MARTINI water in a 10 x 10 x 10 nm box and, after equilibration, was simulated 1  $\mu$ s for production.

To assess the effective free energy as a function of distance between two origami particles, the potential of mean force (PMF) was calculated via umbrella sampling methods using a series of separate simulations in which one adsorbed origami was constrained at a given distance from the other using a harmonic restraint on the xy-coordinates with a spring constant of 50 kJ mol<sup>-1</sup> nm<sup>-2</sup>. Each of these simulations ran for 1  $\mu$ s, and the Weighted Histogram Analysis Method was used to calculate the final PMF. All visualizations were generated using PyMOL and plots were generated using R in RStudio<sup>19</sup>.

### **3. RESULTS**

To assess the properties of the simulated hinges, three types of simulations were prepared: an isolated hinge in water, a hinge adsorbed onto a membrane, and two hinges adsorbed onto the same membrane. For each, a set of simulations was run varying the hinge stiffness,  $k_0$ . The following subsections analyze the hinge angle distributions from these simulations and compare the PMFs describing the effective interactions between two hinges adsorbed onto the same membrane.

### 3.1: Hinge stiffness changes the distribution of angles sampled in water

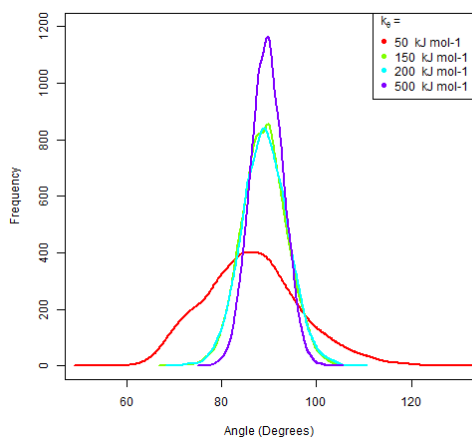


**Figure 2:** Angle distributions for the simulations of hinges in water, ranging from  $k_{\theta} = 50 \text{ kJ mol}^{-1}$  to  $500 \text{ kJ mol}^{-1}$

The hinges simulated in water showed changes in distribution as stiffness changed (Fig. 2). Thermal fluctuations caused the random opening and closing of the hinges, with weaker hinges having a smaller cost in potential energy associated with fluctuations. The stiffer hinges had narrower distributions, while the weaker hinges' distributions were broader. All the distributions centered around the hinges' inherent angle of  $90^{\circ}$ . One deviation from this trend was the  $k_{\theta} = 50 \text{ kJ mol}^{-1}$  case, in which the mean angle was  $86.47^{\circ}$  and the distribution was somewhat asymmetric. The cause of this is unknown.

### 3.2: Hinges adsorbed on a membrane induce membrane curvature and adopt different angles based on stiffness.

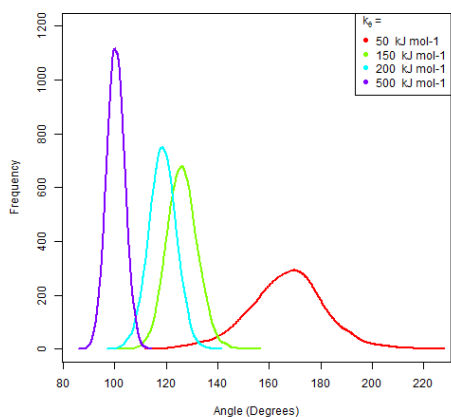


**Figure 3:** Angle distributions for the simulations of hinges adsorbed to a membrane, ranging from  $k_{\theta} = 50 \text{ kJ mol}^{-1}$  to  $500 \text{ kJ mol}^{-1}$

Compared to the angle distributions of the isolated hinges, the distributions of hinges adsorbed to a membrane lost their common centering around the  $90^{\circ}$  equilibrium angle (Fig. 3). Instead, the forces exerted by the membrane onto the hinges change the average angle that a hinge will adopt based on its stiffness. The stiffer hinges were more resistant to bending and had angle distributions centered around more acute angles than the

weaker hinges. Like their behavior in water, the distributions were also narrower in the stiffer hinges than in the weaker ones.

Qualitative assessment of the membrane deformation (*Fig. 4*) shows clear distinction between a weak hinge ( $k_{\theta} = 50 \text{ kJ mol}^{-1}$ ) and stiffer hinges ( $k_{\theta} = 150$  and  $500 \text{ kJ mol}^{-1}$ ). The weak hinge lies almost entirely flatly, inducing essentially no curvature in the membrane, whereas the others retain their angled shape, forcing the membrane to curve. The abilities of the hinge to adopt different angles and deform a membrane differently based on stiffness have interesting implications for nanotechnology. Taking into consideration the hinges designed by Marras et al., which can be tuned to precisely adjust their mechanical properties<sup>14</sup>, and other DNA origami structures that can be induced to deform by outside stimuli<sup>10,15</sup>, we suggest that DNA origami can be used to precisely control local membrane deformation by modulating the inherent angle and stiffness of a hinge-like structure.

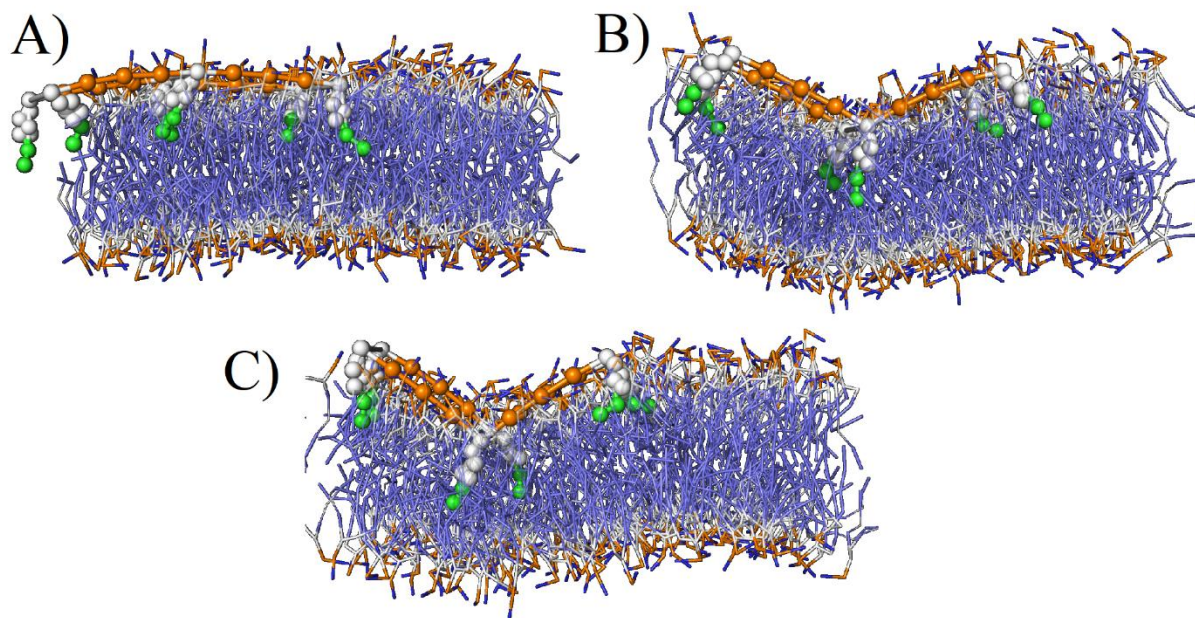


**Figure 4:** Hinges of different stiffnesses inducing different amounts of curvature in the membrane. A)  $k_{\theta} = 50 \text{ kJ mol}^{-1}$ ; B)  $k_{\theta} = 150 \text{ kJ mol}^{-1}$ ; C)  $k_{\theta} = 500 \text{ kJ mol}^{-1}$

### 3.3: Two hinges adsorbed on a membrane align with each other at high stiffness

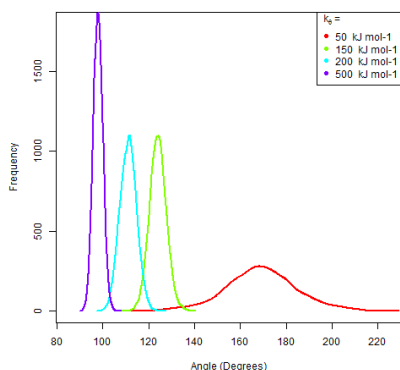


**Figure 6:** Angle distributions for the simulations of two hinges adsorbed to the same membrane, ranging from  $k_\theta = 50 \text{ kJ mol}^{-1}$  to  $500 \text{ kJ mol}^{-1}$

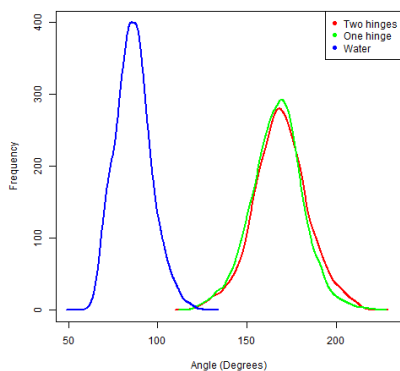


**Figure 7:** Angle distributions for all three cases at  $k_\theta = 50 \text{ kJ mol}^{-1}$

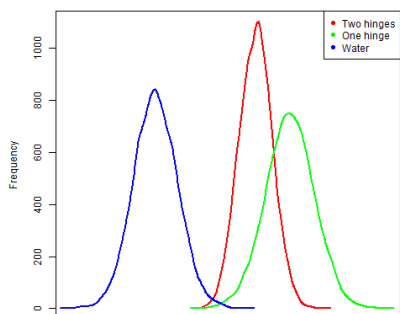


**Figure 5:** Angle distributions for all three cases at  $k_\theta = 200 \text{ kJ mol}^{-1}$

The angle distributions of the hinges in the two-hinge case (Fig. 5) take a similar shape to the distributions in the one-hinge case (Fig. 4), but at slightly more acute angles and narrower distributions for every stiffness apart from  $k_\theta = 50 \text{ kJ mol}^{-1}$ . More can be elucidated from comparing the three different simulation cases of a single hinge stiffness. For the  $k_\theta = 50 \text{ kJ mol}^{-1}$  simulations, it is evident that the hinge being adsorbed to a bilayer makes a difference in the angle distribution compared to when the hinge is in water, but there is no apparent difference between the one and two-hinge cases' distributions (Fig. 6). For the  $k_\theta = 200 \text{ kJ mol}^{-1}$  simulations, the distinction between the hinge-in-water angle distributions and the distributions of the other simulations is still present (Fig. 7). However, there is a new distinction between the one and two-hinge cases that was not present at  $k_\theta = 50 \text{ kJ mol}^{-1}$ . Compared to the one-hinge case, the angle distribution is narrower and centered at a more acute average angle in the two-hinge case. Drawing from the visualizations in Fig. 4, one recognizable difference between the  $k_\theta = 50 \text{ kJ mol}^{-1}$  cases and the other stiffness cases is the lack of

membrane bending in the former. Deformations in the membrane caused by one hinge could be allowing the other hinge to adopt an angle closer to the  $90^\circ$  equilibrium angle. This could mean that the two hinges are favorably aligning near each other in the higher stiffness cases.

Analysis of stiff ( $k_\theta = 200 \text{ kJ mol}^{-1}$ ) and weak ( $k_\theta = 50 \text{ kJ mol}^{-1}$ ) hinges as they diffuse across the membrane (Fig. 8) show that the stiff hinges, once they encountered each other, lined up and remained together for as long as they were simulated. However, the weak hinges never seemed to exhibit this behavior. A side view of this same snapshot confirms a lack of curvature in the membrane with weak hinges adsorbed, but significant curvature in the membrane with stiff hinges (Fig. 9).

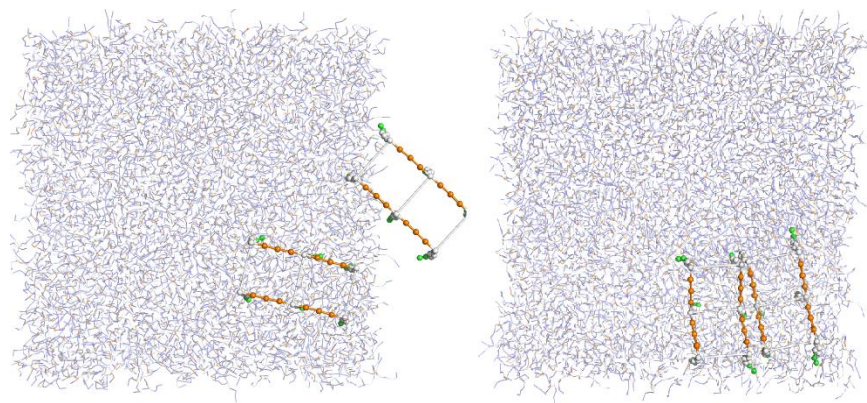


**Figure 9:** On the left, two hinges at  $k_\theta = 50 \text{ kJ mol}^{-1}$  are unaligned. On the right, two hinges at  $k_\theta = 200 \text{ kJ mol}^{-1}$  have positioned themselves very near to each other, becoming aligned. After aligning in this simulation, these two hinges never separated. These systems are simulated using periodic boundary conditions, so the hinges may cross over from one boundary to the other. This is occurring in the left image, where the hinge can be seen crossing over the right-side boundary and interacting with the left side of the membrane patch.

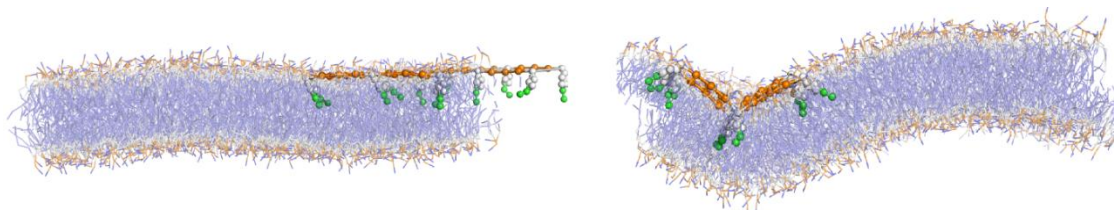


**Figure 8:** On the left, two hinges at  $k_\theta = 50 \text{ kJ mol}^{-1}$  have induced little to no curvature in the membrane and are unaligned. On the right, two hinges at  $k_\theta = 200 \text{ kJ mol}^{-1}$  have produced strong curvature in the membrane and are aligned.

To quantify this effect, PMFs over the distance between the two hinges were calculated for hinges at  $k_\theta = 50, 125, \text{ and } 200 \text{ kJ mol}^{-1}$ . The results are shown below (Fig. 10). While free

energy increases as the distance between hinges decreases in the flexible hinge case ( $k_{\theta} = 50 \text{ kJ mol}^{-1}$ ), the stiff hinge cases ( $k_{\theta} = 125$  and  $200 \text{ kJ mol}^{-1}$ ) show free energy decreasing as the hinges move together, indicating that there is an attraction between the stiff hinges when they get

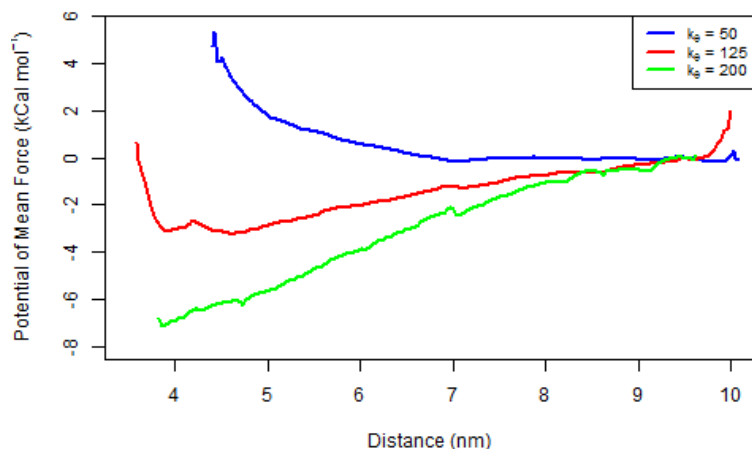


**Figure 10:** PMFs between two hinges over distance for  $k_{\theta} = 50, 125,$  and  $200 \text{ kJ mol}^{-1}$  normalized to  $0 \text{ kcal mol}^{-1}$  at  $9.5 \text{ nm}$ .

close to one another, but there is an opposite, repulsive effect for the weak hinges. This information supports the hypothesis that the stiff hinges will favorably associate with each other when adsorbed onto a membrane, but weak hinges will not. Moreover, this phenomenon

seems to correspond with the hinge's ability to induce curvature in the membrane. This coincides with previous understanding of how membrane particles naturally behave in cell membranes, sculpting membrane curvature to communicate with and recruit other particles<sup>13,19</sup>.

#### 4. CONCLUSION

The ability to incorporate programmable mechanical properties into DNA origami nanoparticles has already shown its potential in many applications, but the capacity of these particles to interact with membranes has not yet been explored. We have demonstrated the ability of DNA origami structures to sculpt membrane curvature in a potentially dynamic way, based on properties of the structures that can be precisely controlled. We have also shown that the membrane deformation induced by origami particles can create conditions

that are favorable for their aggregation, similar to natural membrane-sculpting phenomena within cells. These results imply the potential for a wide range of interesting applications. Tunable or reversible membrane sculpting using DNA origami could be realized with further research. In the short term, fruitful studies could include investigating a reversible locking mechanism for an origami hinge to increase or decrease its stiffness in response to stimuli. Simulated approaches could also benefit from using a larger model than was used in this study. The origami hinges developed by Marras et al. were 100 nm wide, while our model was only 5 nm wide. Exploring the interactions between several of these hinges adsorbed onto the same membrane would also be an interesting future direction.

## REFERENCES

- (1) Zhao, S.; Tian, R.; Wu, J.; Liu, S.; Wang, Y.; Wen, M.; Shang, Y.; Liu, Q.; Li, Y.; Guo, Y.; Wang, Z.; Wang, T.; Zhao, Y.; Zhao, H.; Cao, H.; Su, Y.; Sun, J.; Jiang, Q.; Ding, B. A DNA Origami-Based Aptamer Nanoarray for Potent and Reversible Anticoagulation in Hemodialysis. *Nat Commun* **2021**, *12* (1), 358. <https://doi.org/10.1038/s41467-020-20638-7>.
- (2) Jo, S.; Kim, T.; Im, W. Automated Builder and Database of Protein/Membrane Complexes for Molecular Dynamics Simulations. *PLoS ONE* **2007**, *2* (9), e880. <https://doi.org/10.1371/journal.pone.0000880>.
- (3) Arora, A. A.; de Silva, C. Beyond the Smiley Face: Applications of Structural DNA Nanotechnology. *Nano Reviews & Experiments* **2018**, *9* (1), 1430976. <https://doi.org/10.1080/20022727.2018.1430976>.
- (4) Lee, J.; Patel, D. S.; Stähle, J.; Park, S.-J.; Kern, N. R.; Kim, S.; Lee, J.; Cheng, X.; Valvano, M. A.; Holst, O.; Knirel, Y. A.; Qi, Y.; Jo, S.; Klauda, J. B.; Widmalm, G.; Im, W. CHARMM-GUI *Membrane Builder* for Complex Biological Membrane Simulations with Glycolipids and Lipoglycans. *J. Chem. Theory Comput.* **2019**, *15* (1), 775–786. <https://doi.org/10.1021/acs.jctc.8b01066>.
- (5) Jo, S.; Lim, J. B.; Klauda, J. B.; Im, W. CHARMM-GUI Membrane Builder for Mixed Bilayers and Its Application to Yeast Membranes. *Biophysical Journal* **2009**, *97* (1), 50–58. <https://doi.org/10.1016/j.bpj.2009.04.013>.
- (6) Wu, E. L.; Cheng, X.; Jo, S.; Rui, H.; Song, K. C.; Dávila-Contreras, E. M.; Qi, Y.; Lee, J.; Monje-Galvan, V.; Venable, R. M.; Klauda, J. B.; Im, W. CHARMM-GUI *Membrane Builder* toward Realistic Biological Membrane Simulations. *J. Comput. Chem.* **2014**, *35* (27), 1997–2004. <https://doi.org/10.1002/jcc.23702>.
- (7) Jo, S.; Kim, T.; Iyer, V. G.; Im, W. CHARMM-GUI: A Web-Based Graphical User Interface for CHARMM. *J. Comput. Chem.* **2008**, *29* (11), 1859–1865. <https://doi.org/10.1002/jcc.20945>.
- (8) Brooks, B. R.; Brooks, C. L.; Mackerell, A. D.; Nilsson, L.; Petrella, R. J.; Roux, B.; Won, Y.; Archontis, G.; Bartels, C.; Boresch, S.; Caflisch, A.; Caves, L.; Cui, Q.; Dinner, A. R.; Feig, M.; Fischer, S.; Gao, J.; Hodoseck, M.; Im, W.; Kuczera, K.; Lazaridis, T.; Ma, J.; Ovchinnikov, V.; Paci, E.; Pastor, R. W.; Post, C. B.; Pu, J. Z.; Schaefer, M.; Tidor, B.; Venable, R. M.; Woodcock, H. L.; Wu, X.; Yang, W.; York, D. M.; Karplus, M. CHARMM: The Biomolecular Simulation Program. *J. Comput. Chem.* **2009**, *30* (10), 1545–1614. <https://doi.org/10.1002/jcc.21287>.
- (9) Udomprasert, A.; Kangsamaksin, T. DNA Origami Applications in Cancer Therapy. *Cancer Sci* **2017**, *108* (8), 1535–1543. <https://doi.org/10.1111/cas.13290>.
- (10)

- Han, D.; Pal, S.; Liu, Y.; Yan, H. Folding and Cutting DNA into Reconfigurable Topological Nanostructures. *Nature Nanotech* **2010**, *5* (10), 712–717.  
<https://doi.org/10.1038/nnano.2010.193>. (11)
- Rothemund, P. W. K. Folding DNA to Create Nanoscale Shapes and Patterns. *Nature* **2006**, *440* (7082), 297–302. <https://doi.org/10.1038/nature04586>. (12)
- Bauer, P.; Hess, B.; Lindahl, E. GROMACS 2022.1 Manual. **2022**.  
<https://doi.org/10.5281/ZENODO.6451567>. (13)
- Franquelim, H. G.; Khmelinskaia, A.; Sobczak, J.-P.; Dietz, H.; Schwille, P. Membrane Sculpting by Curved DNA Origami Scaffolds. *Nat Commun* **2018**, *9* (1), 811.  
<https://doi.org/10.1038/s41467-018-03198-9>. (14)
- Marras, A. E.; Zhou, L.; Su, H.-J.; Castro, C. E. Programmable Motion of DNA Origami Mechanisms. *Proc. Natl. Acad. Sci. U.S.A.* **2015**, *112* (3), 713–718.  
<https://doi.org/10.1073/pnas.1408869112>. (15)
- Ke, Y.; Meyer, T.; Shih, W. M.; Bellot, G. Regulation at a Distance of Biomolecular Interactions Using a DNA Origami Nanoactuator. *Nat Commun* **2016**, *7* (1), 10935.  
<https://doi.org/10.1038/ncomms10935>. (16)
- Marrink, S. J.; Risselada, H. J.; Yefimov, S.; Tieleman, D. P.; de Vries, A. H. The MARTINI Force Field: Coarse Grained Model for Biomolecular Simulations. *J. Phys. Chem. B* **2007**, *111* (27), 7812–7824. <https://doi.org/10.1021/jp071097f>. (17)
- Amir, Y.; Ben-Ishay, E.; Levner, D.; Ittah, S.; Abu-Horowitz, A.; Bachelet, I. Universal Computing by DNA Origami Robots in a Living Animal. *Nature Nanotech* **2014**, *9* (5), 353–357.  
<https://doi.org/10.1038/nnano.2014.58>. (18)
- Simunovic, M.; Šarić, A.; Henderson, J. M.; Lee, K. Y. C.; Voth, G. A. Long-Range Organization of Membrane-Curving Proteins. *ACS Cent. Sci.* **2017**, *3* (12), 1246–1253.  
<https://doi.org/10.1021/acscentsci.7b00392>. (19)
- The PyMOL Molecular Graphics System, Version 2.0 Schrödinger, LLC.